Georgantzia E, Pichowski J, Aminulai O, Crump D and Kashani MM (2025) Experimental Investigation of Nonlinear Cyclic Flexural Behaviour of Hollow and Concrete-Filled Aluminium Beams. ASCE Journal of Structural Engineering. 151(11): https://doi.org/10.1061/JSENDH.STENG-14937

Experimental investigation of nonlinear cyclic flexural behaviour of hollow and concrete-filled aluminium beams

Dr Evangelia Georgantzia

Lecturer in Engineering

Email: evangelia.georgantzia@city.ac.uk

Address: Tait Building, Department of Engineering, School of Science & Technology, City St George's, University of London, Northampton Square, EC1V 0HB, London, United Kingdom

Mr Joshua Pichowski

Undergraduate Student

Email: jhp1g21@soton.ac.uk

Address: Building 178, Boldrewood Innovation Campus, School of Engineering, Faculty of Engineering and Physical Sciences, University of Southampton, Southampton, SO16 7QF, United Kingdom

Dr Hammed O. Aminulai

Research Associate

Email: h.o.aminulai@soton.ac.uk

Address: Building 178, Boldrewood Innovation Campus, School of Engineering, Faculty of Engineering and Physical Sciences, University of Southampton, Southampton, SO16 7QF, United Kingdom

Dr Duncan Crump

Principal Experimental Officer

Email: d.a.crump@soton.ac.uk

Address: Large-Scale Structural Testing Laboratory (LSTL), Building 178, Boldrewood Innovation Campus, School of Engineering, Faculty of Engineering and Physical Sciences, University of Southampton, Southampton, SO16 7QF, United Kingdom

Dr Mohammad M. Kashani

Associate Professor in Civil Engineering

Email: mehdi.kashani@soton.ac.uk

Address: Room 4019, Building 178, Boldrewood Innovation Campus, School of Engineering, Faculty of Engineering and Physical Sciences, University of Southampton, Southampton, SO16 7QF, United Kingdom

Experimental investigation of nonlinear cyclic flexural behaviour of hollow and concrete-filled aluminium beams

E. Georgantzia, J. Pichowski, H.O. Aminulai, D. Crump and M. M. Kashani

Abstract

This study presents an experimental programme to characterise, for the first time, the nonlinear cyclic flexural behaviour of hollow and concrete-filled aluminium tubular beams at large rotation levels up to 0.08 rad. Particularly, four different tubular cross-sections, fabricated from two grades of structural aluminium alloys –6082-T6 and 6063-T6– with various cross-sectional slenderness were tested with and without concrete infill to establish their hysteretic flexural behaviour. All tested specimens showed hysteretic loops without significant gradual strength and stiffness degradation under cyclic loading. The influence of aluminium alloy type, cross-sectional slenderness and presence of concrete infill on the plastic hinge deformation, ultimate strength, failure mode, secant stiffness degradation and energy dissipation capacity is thoroughly investigated. Analysis of the in-plane strain measurements from Digital Image Correlation suggest that under large cyclic loads the examined members can develop an average plastic hinge length equal to 1.5 times the largest cross-sectional dimension measured from the fixed end of the members. Overall, the experimental results demonstrate that hollow and concrete-filled aluminium beam members can sustain large deformations without any structural damage under large rotation levels.

Introduction

Steel hollow cross-sections are highly versatile and widely used in truss and frame systems for both structural and architectural purposes owing to their beneficial properties. These include high structural efficiency under compression, torsion, and bending, easy and quick connection of structural components and aesthetic appearance. Aluminium is an increasingly viable alternative to steel in structural applications due to its exceptional properties. It is roughly two-thirds lighter than steel, offering a high strength-to-weight ratio that makes it ideal for projects in which the weight is a primary design concern including aerospace structures, automotive and rail transportation, modular construction, and lightweight bridges. In these applications, reducing weight is crucial for improving efficiency, performance, and fuel economy, as well as simplifying transportation and assembly. Further to this, in seismic-prone zones, aluminium unlike steel, can satisfy the required strength and ductility requirements without a weight penalty (Georgantzia and Kashani 2024). The natural corrosion resistance of aluminium enhances durability, reducing maintenance

requirements and extending the lifespan of structures in harsh environments, such as marine and industrial settings. Its excellent workability allows for complex shapes and custom designs through processes such as extrusion. Although the initial material cost is higher compared to steel, the benefits of reduced weight, durability, and recyclability often offset this in the long term (Georgantzia and Kashani 2024). These advantages make aluminium a compelling material choice for innovative structural designs. However, the low modulus of elasticity of aluminium –approximately one-third that of steel– may cause failure due to inward local buckling. To prevent or delay the occurrence of inward local buckling, researchers have suggested filling aluminium hollow sections with concrete or green concrete (Feng et al. 2017; Chen et al. 2018; Georgantzia et al. 2021a; Ali et al. 2022; Gkantou et al. 2023). This approach leverages the benefits of both materials to achieve high performance by increasing stiffness and strength.

Most studies on aluminium hollow sections have primarily focused on evaluating their structural behaviour under monotonic loading, examining various frame components such as beams, columns, connections, and joints (Zhu and Young 2009; Su et al. 2014; Castaldo et al. 2017; Piluso et al. 2019; Bock et al. 2021; Georgantzia et al. 2022a). The results of these studies clearly demonstrate the potential of aluminium as a primary structural material for civil engineering applications. They also improve confidence in the prediction of structural behaviour and assessment of relevant codification rules included in the European standard EN 1999-1-1 (CEN 2023a) and the American Aluminium Design Manual (ADM) (AA 2020). For concrete-filled aluminium sections, the existing studies are limited and focus solely on their structural performance under monotonic loading (Chen et al. 2017; Feng et al. 2017; Georgantzia and Gkantou 2021; Georgantzia et al. 2021a, 2022b; Ali et al. 2022). Currently, EN 1999-1-1 (CEN 2023a) and ADM (AA 2020) do not provide design guidelines for structures with this type of composite sections.

Recently, Nastri et al. (2025) presented the first tests on the cyclic behaviour of aluminium beams under non-uniform bending. The beams comprised 4 square hollow sections made from 6060-T66 alloy, with two different lengths namely 1000 mm and 1300 mm. The beams were subjected to three-point bending cyclic tests and the results were utilised to develop a detailed finite element model in ABAQUS (Dassault Systèmes Simulia Corp.), able to precisely capture the fracture of the beams. Despite this significant paucity in the literature, which limits our understanding on the seismic performance of aluminium members, dedicated rules for the seismic design of aluminium structures are given in Chapter 15 of the latest draft of the Second Generation of EN1998-1-2 (CEN 2022). It is noteworthy that these rules are mainly based on the Japanese standards for the seismic design of aluminium structures

developed by the Architectural Institute of Japan (AIJ 2003), and the European standards for seismic design of carbon steel structures included in EN1998-1-2 (CEN 2022). On the other hand, ADM (AA 2020) does not provide design guidelines for seismic design of aluminium structures. Considering the fundamental mechanical differences between aluminium and carbon steel, there is a need to investigate the seismic performance of aluminium members before they can be safely used in seismic-prone zones (Georgantzia et al. 2024). Moreover, there is no detailed study on concrete-filled aluminium sections under cyclic loading, which indicates an urgent need for further research in this area.

Research contribution and novelty

The current study aims to provide, for the first time, a detailed experimental investigation of the flexural behaviour of hollow and concrete-filled aluminium tubular cross-sections under large cyclic loads. To this end, an experimental campaign including 8 tests was performed at the National Infrastructure Laboratory at the University of Southampton to characterise the nonlinear cyclic flexural behaviour of 6082-T6 and 6063-T6 tubular cross-sections with and without concrete infill at large rotation levels up to 0.08 rad. The 6082-T6 grade represents a typical high strength heat-treated aluminium alloy (Georgantzia et al. 2022b), whilst 6063-T6 grade represents a typical normal strength aluminium alloy (Georgantzia et al. 2022b). 6082-T6 is often referred to as a 'structural alloy' and has been used predominantly in highly stressed applications such as roof trusses and bridges (Georgantzia et al. 2022b). 6063-T6 is often referred to as an architectural alloy and offers high corrosion resistance (Georgantzia et al. 2022b). The influence of aluminium alloy type, cross-sectional slenderness and presence of concrete infill on the plastic hinge deformation, ultimate strength, failure mode, secant stiffness degradation and energy dissipation capacity is thoroughly investigated. Furthermore, the experimental results are utilised to evaluate the limitations of Chapter 15 in the latest draft of the Second Generation of EN1998-1-2 (CEN 2022) regarding alloys and cross-section classes allowed for dissipative aluminium members in bending.

Experimental programme

Test specimens

An experimental programme was performed to evaluate the major-axis flexural behaviour of hollow and concrete-filled aluminium cross-sections under cyclic loading. A total of 8 tests were carried out, including 4 hollow and 4 concrete-filled aluminium beam members. The specimens comprised rectangular and square tubular cross-sections fabricated from two aluminium alloy types namely 6082-T6 and 6063-T6. Table 1 summarises the detailed information of the test specimens, where D is the outer depth, B is the outer width and t is the wall thickness. The adopted notation is also shown in Fig. 1. It is noted that the tested cross-sections are small for use as primary flexural members in typical building applications. However, they represent some of the largest commercially available extruded tubular profiles in the current aluminium industry in the UK. The designation of the specimens is defined according to the alloy type, nominal geometric dimensions and the presence of concrete infill. For example, the label "H152.4×50.8×6.35-C" indicates a beam of high-strength alloy 6082-T6 with nominal depth of 152.4 mm, nominal width of 50.8 mm and nominal thickness of 6.35 mm. The letter (-C) of the label signifies the presence of concrete infill. If the column label starts with the letter (-N), it denotes that the specimen is of normal strength alloy 6063-T6. The cross-sectional dimensions were selected to cover various aspect ratios D/B and slenderness parameters b/t (where $b=B-2t$ is the flat width of the wall under compression). Particularly, the chosen b/t were ranging from 5.98 to 21.36. These values enabled to examine the major-axis flexural behaviour of the hollow and concrete-filled aluminium sections across Classes 1-3 according to EN 1999-1-1 (CEN 2023a). According to ADM (AA 2020), cross-sections are classified based on their limit state; yielding, inelastic buckling and elastic buckling. Herein, the limit state of the considered cross-sections based on ADM (AA 2020) is either yielding or inelastic buckling (see Table 1). It is noteworthy that the ADM (AA 2020) classification system is less refined than that of EN 1999-1-1 (CEN 2023a) and there is no distinction between cross-sections where the full exploitation of the material hardening properties is allowed (Class 1 cross-sections in EN 1999-1-1 (CEN 2023a)) or prevented by the onset of plastic instability phenomena (Class 2 cross-sections in EN 1999-1-1 (CEN 2023a)). This is attributed to the limited pool of available structural performance data that were utilised in its development. Henceforth, cross-section classes will be referred to in accordance with EN 1999-1-1 (CEN 2023a) classification system.

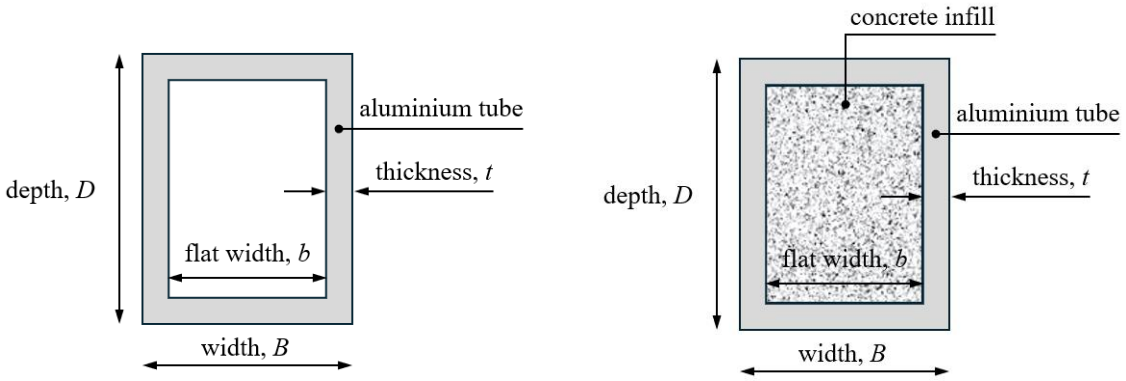

(a) (b)

Fig. 1: Geometric properties of (a) hollow and (b) concrete-filled aluminium cross-sections.

Table 1. Summary of specimen information.

Specimen ID	D (mm)	B (mm)	t (mm)	D/B	b/t	EN 1999-1-1 (CEN 2023a) Class	ADM (AA 2020) Limit state	L_{eff} (mm)
H152.4×50.8×6.35	152.20	50.50	6.33	3.01	5.98	1	Yielding	1080
H152.4×50.8×6.35-C	152.80	50.80	6.28	3.01	6.09	1	Yielding	1060
H101.6×101.6×6.35	101.20	99.80	6.32	1.01	13.79	2	Yielding	1040
H101.6×101.6×6.35-C	101.60	101.10	6.36	1.00	13.90	2	Yielding	1060
N101.6×50.8×3.25	101.50	50.30	3.21	2.02	13.67	2	Yielding	1040
N101.6×50.8×3.25-C	101.60	51.10	3.23	1.99	13.82	2	Yielding	1050
N76.2×76.2×3.25	76.40	76.40	3.27	1.00	21.36	3	Inelastic buckling	1060
N76.2×76.2×3.25-C	76.00	76.80	3.29	0.99	21.34	3	Inelastic buckling	1060

6082-T6 and 6063-T6 alloys: Tensile coupon tests

A series of tensile tests were conducted on flat coupons to determine the mechanical properties of the 6082-T6 and 6063-T6 alloys. For each examined cross-section, flat coupons were cut and machined in line with the geometric requirements described in EN ISO 6892-1 (CEN 2019a). Upon machining, each coupon was placed between the jaws of a 100 kN Instron testing machine and was subjected to monotonic tensile loading with 0.2 mm/min displacement rate up to fracture. Moreover, a calibrated extensometer with gauge length of 50 mm was mounted onto the central necked part of each coupon to measure the longitudinal strains during testing. In total, 13 coupons were tested for each alloy. Table 2 reports the mean and coefficient of variation (COV) values of the measured material properties. The measured material properties include the initial modulus of elasticity E, the 0.1 % proof stress $\sigma_{0.1}$, the 0.2 % proof stress $\sigma_{0.2}$, the ultimate tensile stress σ_u, the strain corresponding to ultimate tensile stress ε_u, the strain at fracture ε_f

and the strain hardening exponent n (Hill et al. 1960; Ramberg and Osgood 1943). Fig. 2 illustrates typical experimental stress-strain (σ–ε) curves for the 6082-T6 and 6063-T6 alloys. From Fig. 2, it can be seen that the stress–strain curves of both examined alloys exhibit different degrees of nonlinearity, roundedness in the region of the $\sigma_{0.2}$ and strain hardening, primarily due to their slightly different chemical composition. The mean and COV values of $\sigma_u/\sigma_{0.2}$, defined as strain hardening ratio, are also included in Table 2. These values indicate that the 6063-T6 alloy exhibits more pronounced strain-hardening behaviour, as its $\sigma_u/\sigma_{0.2}$ ratio is 120%, compared to 108% for the 6082-T6 alloy.

Table 2. Mean measured material properties of 6082-T6 and 6063-T6 alloys.

	E (MPa)	$\sigma_{0.1}$ (MPa)	$\sigma_{0.2}$ (MPa)	σ_u (MPa)	ε_u (%)	ε_f (%)	n	$\sigma_u/\sigma_{0.2}$
				6082-T6				
Mean	67653	295.0	299.3	322.5	7.6%	11.5%	49.9	1.08
COV	0.03	0.02	0.02	0.01	0.04	0.15	0.20	0.01
				6063-T6				
Mean	69309	207.4	212.0	253.5	10.3%	13.0%	32.9	1.20
COV	0.14	0.02	0.02	0.02	0.10	0.14	0.23	0.00

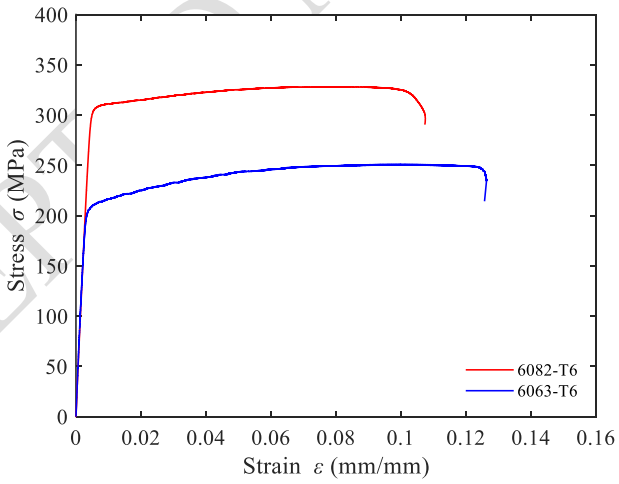

Fig. 2: Typical stress-strain curves obtained from the tensile coupon tests.

Concrete infill: Compressive cube tests

A ready-mixed high strength concrete made of cement, graded sand and 10 mm maximum coarse aggregate size was used to fill the concrete-filled aluminium beam members. The concrete mixture had a 28-day target compressive

cube strength of 50 MPa. A drum mixer was used to blend the concrete mix and clean water until the required consistency and slump according to (CEN 2019b), was achieved. For each batch of concrete mixture, three 100 mm × 100 mm × 100 mm standard concrete cubes were cast and kept in rest period for 24 hours. After removal of mould, the cubes were immersed in water at room temperature for curing. The concrete cubes were subjected to compression testing the same day of each performed beam test resulting in average compressive cube strength of 58.39 MPa (48.39 MPa corresponding cylinder strength according to EN 1992-1-1 (CEN 2004)) with a COV value of 0.13.

Specimen preparation

All beam specimens were designed to have the same length. In preparing the specimens, aluminium tubes were cut to length of 1500 mm and then were milled flat at the bottom surface to a tolerance of ±0.02 mm to prevent any instability due to unwanted movement or tilting. The tubes for the concrete-filled specimens, were supported vertically and filled with concrete which was compacted by an electric vibrator to prevent any void in the specimens. Upon casting, the concrete-filled specimens were left to cure for 28 days before the execution of the structural testing.

Instrumentation and test setup

Fig. 3a shows a schematic illustration of the test setup along with the employed instrumentation, and Fig. 3b shows a photograph of a typical test. Each hollow and concrete-filled beam specimen was vertically cantilevered, with a pinned top end and a fully fixed bottom end. This arrangement allowed for evaluation of the hysteretic flexural and formation of the plastic hinge at the beam end as expected for a beam member in a seismic moment frame system. Each beam specimen was placed carefully on the rigid base and accurately centred. The bottom end of the specimen was sandwiched between two large steel angles, connected by seven high-strength bolts; three passing through the specimen itself and four positioned on either side of the specimen. The steel angles were then anchored to the rigid base using eight bolts each, which passed through slotted holes. For the hollow specimens, wooden blocks with dimensions equal to the internal ones of the cross-sections were inserted at the bottom of the tubes to ensure that the inelastic deformations occurred outside of the connection region. An MTS servo-hydraulic actuator with 250 kN capacity was used to apply lateral displacement at the top of the specimen controlled by a Flextest 200 controller running AeroPro software. The actuator was connected to the top of the specimen using two 20-mm-thick steel plates and four high-strength bolts, which were tightened prior to testing to eliminate any gap between the specimen and the

actuator. The effective length L_{eff} of each specimen, defined as the distance between the actuator's centroid and the tip of the angle, is listed in Table 1.

Each specimen was instrumented to capture the lateral deflections and deformation behaviour within the plastic hinge region, while also providing a detailed information on the inelastic flexural behaviour under cyclic loading. Three equally spaced linear variable displacement transducers (LVDTs) were placed along the length of the specimen to measure its lateral deflection. The material strain was measure using eight linear electrical resistance strain gauges with 5% strain limit, attached at two cross-sections located 10 mm and 2D mm distance from the tip of the steel angles as shown in Fig. 3a. Specifically, two strain gauges were affixed to each outer face in the loading direction, positioned 10 mm from the centreline of the cross-section width. Additionally, a 2D Digital Image Correlation (DIC) was employed to measure in-plane strain and local deformations, full-field, within the expected plastic hinge region. The DIC setup used a single camera aligned perpendicular to the test sample capturing with lens and stand-off to provide a field of view encompassing the entire speckled region indicated on the schematic in Fig. 3a. The images were processed using MatchID software, Gent, Belgium, with each deformed image correlated to the reference image. Details about the camera, settings and parameters that were used in the DIC are presented in Table 3. The applied load was measured using the actuator load cell, while a data acquisition system with a sampling frequency of 10 Hz recorded the applied load, lateral deflection and strains.

Table 3. Cameras, settings, and parameters used in DIC.

Sensor and digitization	CCD* 2,456×2,058 pixels, 8-bit
Exposure time and recording rate	190,00 μs, 1 Hz
Mean camera noise (% of dynamic range)	0.0037%, 0.0034%
Lens and imaging distance	Nikkor 50 mm, 1.68 m
Number of images averaged for resolution calculation	2
Pixel size	5.55 μm
Subset, step	57, 29 pixels
Correlation criterion, Interpolation, Shape function	NSSD, Local Bicubic Spline, Affine
Prefiltering	Gaussian
Smoothing technique	None
Virtual strain gauge	173 pixels
Mean strain resolution	338 με

*CCD=Charged-coupled device

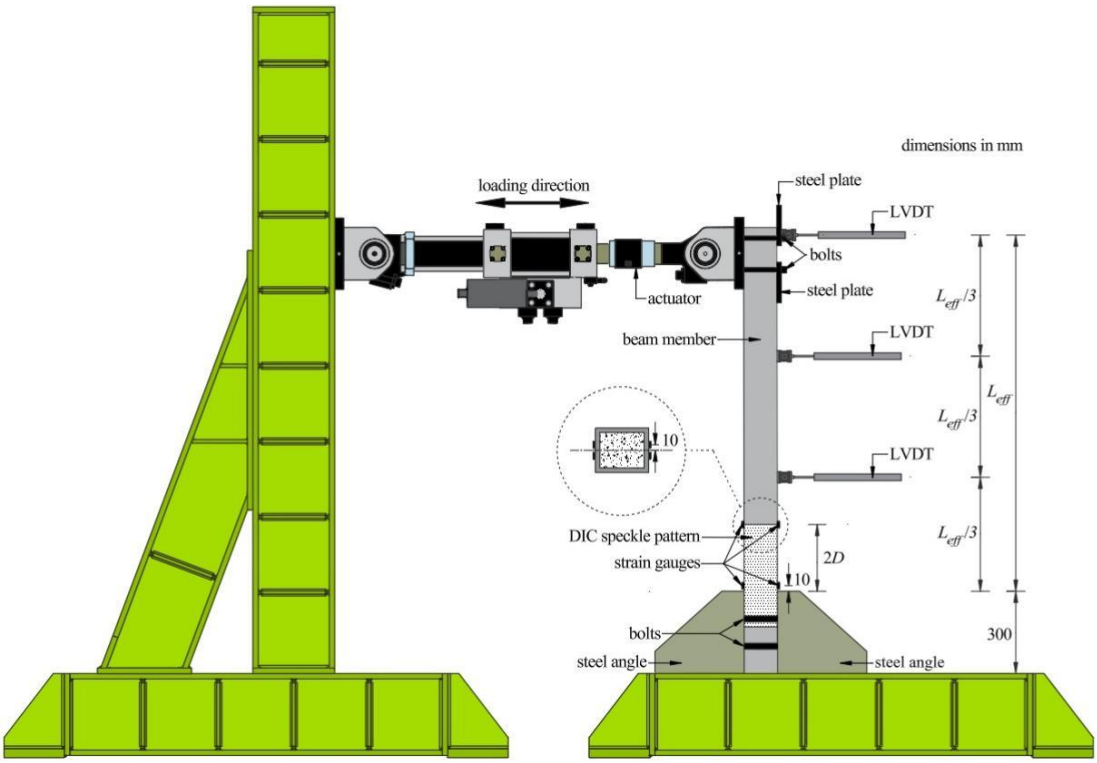

(a)

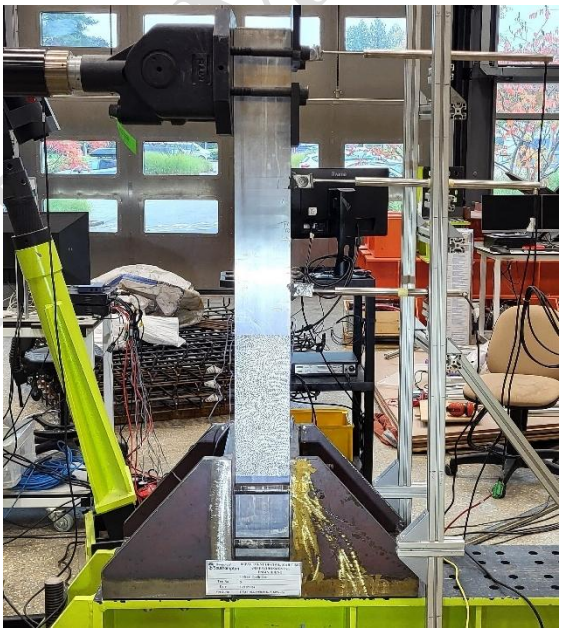

(b)

Fig. 3: (a) Schematic illustration of the test setup and instrumentation and (b) Photograph of a typical beam test.

Loading protocol

A standard cyclic symmetric lateral loading protocol, adapted from the SAC (far field) loading history (Krawinkler et al. 2000), was employed (see Fig. 4). This protocol uses the yield displacement $\delta_{0.2}$ as a reference for increasing the amplitude of the cycles. The loading history consists of two cycles applied at $0.15\delta_{0.2}$, $0.30\delta_{0.2}$, $0.45\delta_{0.2}$, $0.60\delta_{0.2}$, $0.85\delta_{0.2}$ and $1.0\delta_{0.2}$, followed by pairs of cycles with amplitudes increasing in increments of $0.15\delta_{0.2}$ until either $3\delta_{0.2}$ (corresponding to chord rotation θ roughly 0.08 rad) is achieved, or failure occurs. The yield displacement $\delta_{0.2}$ was estimated to be 29.70 mm, calculated as the ratio $\theta_{0.2}/L_{eff}$, where $\theta_{0.2}$ is the yield chord rotation determined using the Eq. from (Araújo and Castro 2016):

$$\theta_{0.2} = M_{pl} L_{eff} / 3EI \tag{1}$$

where M_{pl} is the plastic bending moment calculated by multiplying the $\sigma_{0.2}$ with the plastic section modulus W_{pl}, and EI is the flexural rigidity of the beam specimen.

It is noted that lateral displacement in the direction away from and towards the reaction frame was considered as positive and negative, respectively.

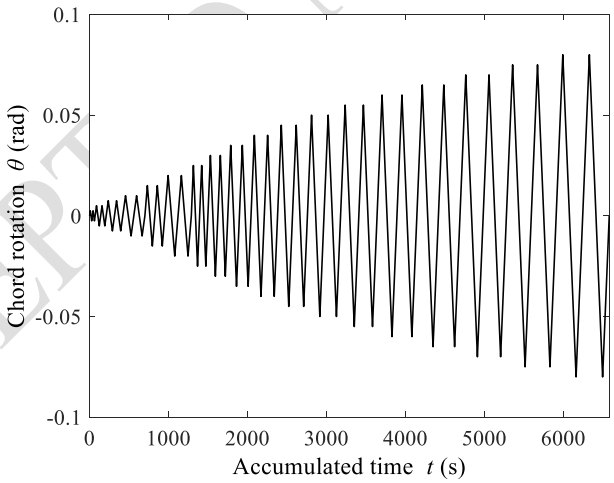

Fig. 4: Loading protocol.

Experimental results and discussion

Nonlinear cyclic response of hollow aluminium beam members (component response)

General observations

Figs. 5-8 present the nonlinear cyclic response of all hollow aluminium beam members as force–displacement (F–δ) and moment–chord rotation (M–θ) curves. It is noted that the rotation was calculated as the ratio of the applied lateral displacement δ to cantilever length L_{eff}. The envelope curves are also shown in Figs. 5-8, which were obtained by connecting the peak point of the first cycle of each applied amplitude on the hysteretic curves. Moreover, a photograph for each specimen at the completion of the test is included in these figures. Each specimen was tested until the maximum θ value of 0.08 rad or complete failure. Overall, yielding initiated between 0.023 rad and 0.051 rad depending on the alloy type and cross-section size, and damage was localised at the bottom end of the specimens mainly in the vicinity of the top hole. The specimens sustained significant deformations and once the inelastic local strain demands exceeded the ε_f –at θ between 0.064 rad and 0.081 rad–, the tube fractured. It is noteworthy that the connection at the bottom end of the specimens did not provide fully fixed conditions. Consequently, a larger elastic rotation compared to the theoretical cantilever beam was observed. All tested specimens displayed hysteretic loops without significant gradual strength degradation under cyclic loading, which is a desirable behaviour for structural members in seismic design. Moreover, the tested specimens showed relatively good symmetry with respect to positive and negative loading, indicating stable behaviour in either direction. It was also observed that the second cycle of each θ demand level exhibited minimal cyclic degradation, closely resembling the response observed in the initial cycle. Finally, the experimental results revealed that as soon as the first crack appeared on one side of the beam, a sudden drop in strength occurred, followed by complete fracture, indicating a brittle failure mode. However, this happened during the second repeated cycle at a rotation beyond 0.06 rad, which is considered very large. Table 4 summarises the response parameters obtained from the tests, including the maximum lateral force F_{max}, maximum bending moment M_{max}, the displacement δ_{max} corresponding to M_{max} and chord rotation at characteristic points; (a) yielding initiation, $\theta_{0.2}$, (b) corresponding to M_{max}, θ_{max},(c) buckling initiation, θ_b, (d) occurrence of the 1st fracture of the aluminium tube, θ_f and (e) complete collapse –loss of structural integrity and therefore termination of test– or completion of test, θ_{co}.

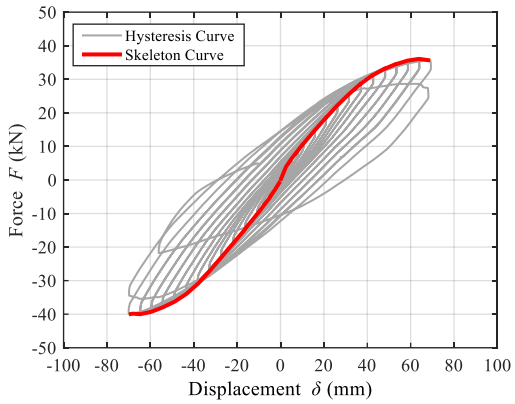

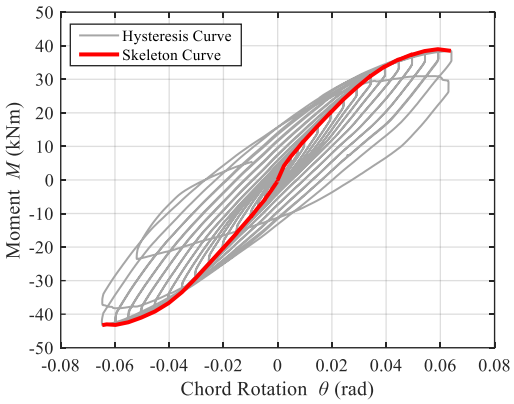

(c) (d) (e)

Fig. 5: Nonlinear cyclic response of the H152.4×50.8×6.35 beam; (a) force-displacement hysteretic curve, (b) moment-chord rotation hysteretic curve and (c) photograph of the specimen at completion of the test.

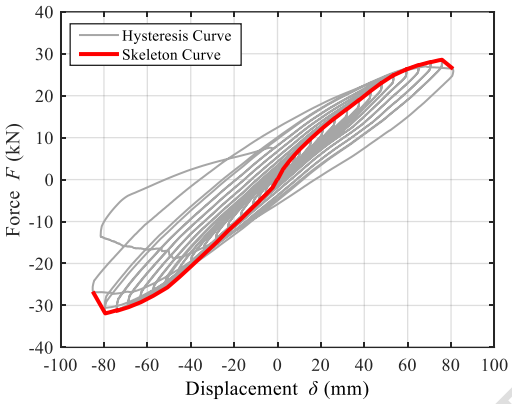

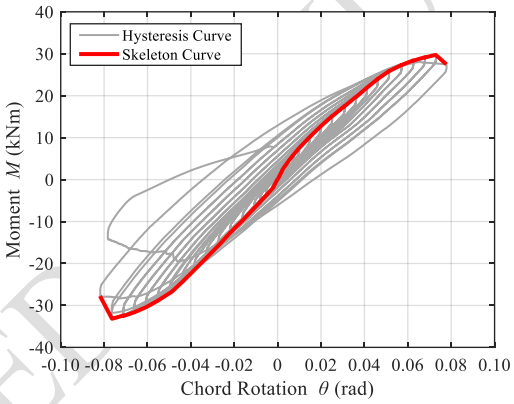

(a) (b) (c)

Fig. 6: Nonlinear cyclic response of the H101.6×101.6×6.35 beam; (a) force-displacement hysteretic curve, (b) moment-chord rotation hysteretic curve and (c) photograph of the specimen at completion of the test.

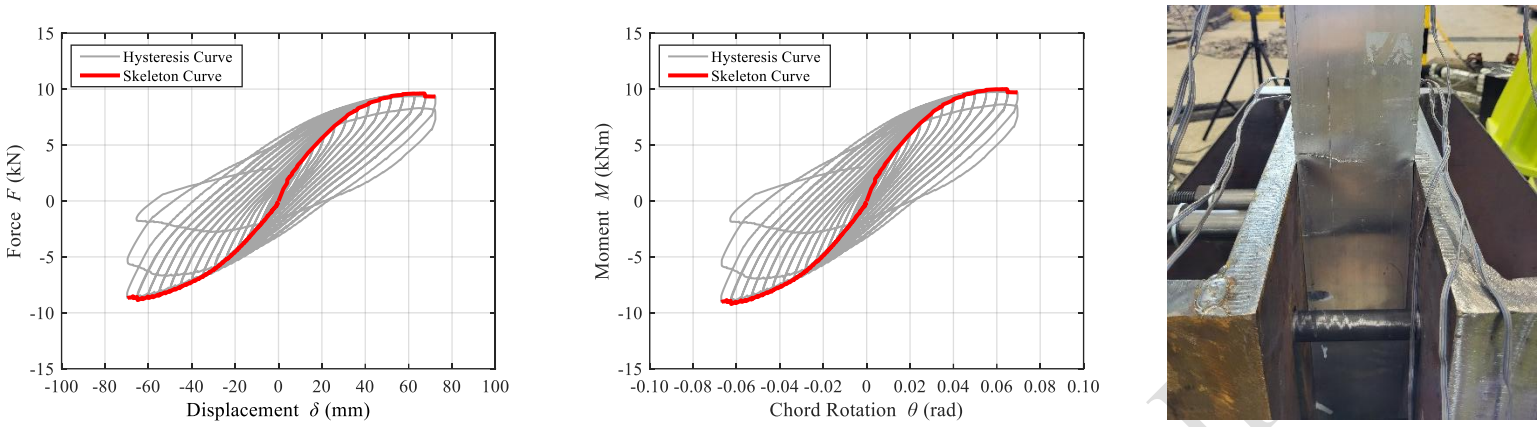

(a) (b) (c)

Fig. 7: Nonlinear cyclic response of the N101.6×50.8×3.25 beam; (a) force-displacement hysteretic curve, (b) moment-chord rotation hysteretic curve and (c) photograph of the specimen at completion of the test.

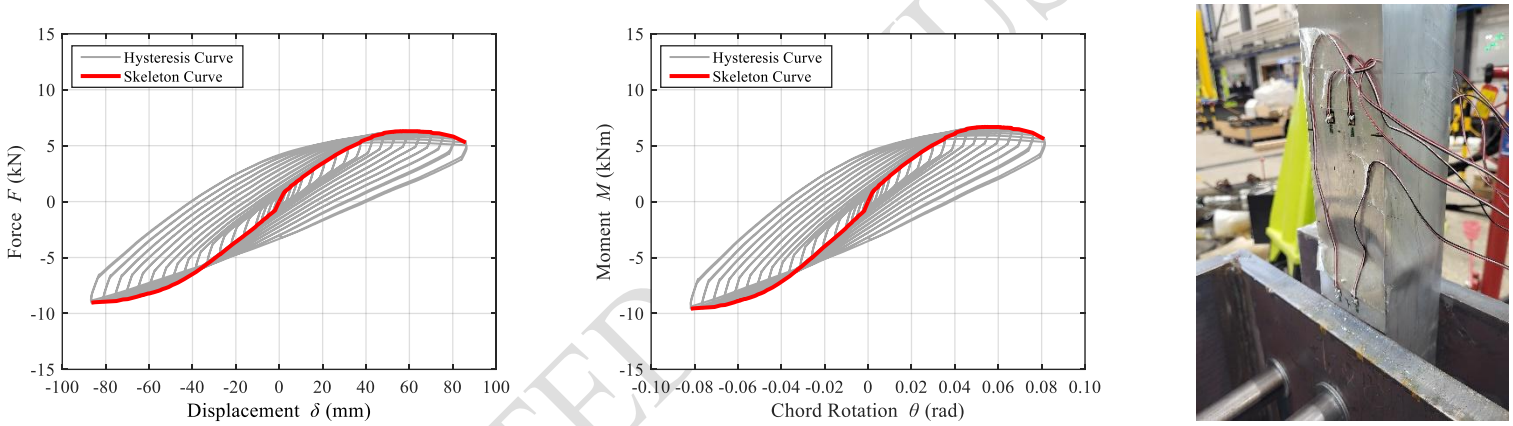

(a) (b) (c)

Fig. 8: Nonlinear cyclic response of the N76.2×76.2×3.25 beam; (a) force-displacement hysteretic curve, (b) moment-chord rotation hysteretic curve and (c) photograph of the specimen at completion of the test.

Classes 1 and 2 6082-T6 cross-sections

The H152.4×50.8×6.35 specimen with section classified as Class 1, reached its M_{max} at -0.060 rad and failed in the subsequent amplitude due to two fractures initiated in the vicinity of the top hole at the flanges and propagated through the webs as shown in Fig. 5(c). The H101.6×101.6×6.35 specimen with Class 2 section, presented a similar failure mechanism with a single fracture at the same location. Comparing H152.4×50.8×6.35 and H101.6×101.6×6.35 specimens that are both fabricated from the same alloy, the former specimen failed at a lower θ as a result of the larger cross-sectional dimensions and hence higher stiffness.

Classes 2 and 3 6063-T6 cross-sections

The N101.6×50.8×3.25 specimen which has Class 2 section, failed similarly to H101.6×101.6×6.35 specimen but at smaller θ. This specimen, which is fabricated by a lower strength alloy, yielded quite earlier and developed higher inelastic longitudinal strains at fracture, ε_f. The N76.2×76.2×3.25 specimen, consisting of Class 3 section, exhibited significant inward local buckling in the flange in the positive direction. Local buckling initiated at 0.056 rad and upon yielding, and propagated through the webs in the form of outward local buckling (see Fig. 8(c)). This resulted in a plateau of the bending moment, in the positive direction, with a minor decrease during later cycles. Conversely, there was no local buckling in the negative direction and thus the bending moment continued increasing to the end of the test.

Comparison of all hollow members

Among all hollow members tested, the H152.4×50.8×6.35 exhibited the highest M_{max}, 43.26 kNm, which is over four times the lowest of 9.58 kNm, observed in the N76.2×76.2×3.25 member. In general, the specimens with larger cross-sectional dimensions and fabricated from high-strength 6082-T6 alloy achieved higher M_{max}.

Implications in design code development

According to Chapter 15 in the latest draft of the Second Generation of EN1998-1-2 (CEN 2022), only Class 1 cross-sections should be used for dissipative aluminium members in bending in ductility class DC2 (medium ductility class) buildings. Moreover, in Chapter 11 which is for seismic design of steel buildings, it is stated that the steel joints should be designed to provide a plastic part of the rotation capacity θ_{pl} of the beam greater than 0.02 rad in DC2. In this study, θ_{pl}, calculated as θ_{co} - $\theta_{0.2}$, at the plastic hinge region of each tested beam member is reported in Table 4. All θ_{pl} values are greater than 0.02 rad showing that the plastic hinge region of the tested beam members provides the required local deformation capacity for DC2 buildings. Therefore, the experimental results show that Class 2 and 3 cross-sections can be used for dissipative aluminium members in bending in DC2 buildings. However, if a fully fixed connection had been provided at the bottom of the specimens, it is expected that stress concentration at the fixed end would have been more significant, potentially leading to earlier crack initiation and propagation. As a result, θ_{co} will be smaller but the exact reduction relative to $\theta_{0.2}$ remains uncertain, as both parameters influence θ_{pl}. For this reason, more research studies are needed to fully verify the abovementioned findings.

Furthermore, the 6082-T6 and 6063-T6 alloys investigated in this study are not listed in Chapter 15 as permitted alloys for dissipative members in DC2 buildings. However, this standard allows for the use of alternative alloys provided that ratio of $\sigma_u/\sigma_{0.2} \geq 1.10$ and $e_f \geq 10\%$. According to Table 2, both alloys satisfy the criterion of $e_f > 10\%$, while $\sigma_u/\sigma_{0.2}$ values are 1.08 and 1.20 for 6082-T6 and 6063-T6, respectively. Although the 6082-T6 alloy marginally does not meet the criterion of $\sigma_u/\sigma_{0.2} \geq 1.10$ in this study, other investigations have shown that it can satisfy this requirement (Georgantzia et al. 2022c, 2023, 2024). This variability arises because the mechanical properties of the alloy depend heavily on its specific chemical composition and fabrication process, which can slightly differ between manufacturers. It is noteworthy that the threshold value of 1.10 for the $\sigma_u/\sigma_{0.2}$ ratio is purely based on the monotonic loading. However, it has been found that structural aluminium exhibits combined kinematic and slight isotropic hardening behaviour when subjected to cyclic loading (Georgantzia et al. 2024). Hence, 6082-T6 and 6063-T6 alloys are suggested to be used for dissipative members in DC2 buildings.

Table 4. Response parameters of the test beam members.

Specimen ID	F_{max} (kN)	F_{max} increase*** (%)	M_{max} (kNm)	$\lvert M_{max}/M_{pl}\rvert$	δ_{max} (mm)	Chord rotation θ at characteristic points					
						Yielding initiation, $\theta_{0.2}$ (rad)	Buckling initiation, θ_b (rad)	Corresponding to M_{max}, θ_{max} (rad)	Fracture occurrence, θ_f (rad)	Complete collapse or Completion of test, θ_{co} (rad)	Plastic rotation, θ_{pl} (rad)
H152.4×50.8×6.35	-40.06	16% (-)*	-43.26	1.34	-64.61	-0.037 (1)**	-	-0.060 (1)	0.064 (2)	-0.065	0.022
H152.4×50.8×6.35-C	-46.65		-49.45	1.38	-75.6	-0.035 (1)	-	-0.071 (1)	0.069 (1)	-0.071	0.029
H101.6×101.6×6.35	-31.90	12% (+)	-33.18	1.31	-79.42	-0.051 (1)	-	-0.076 (1)	-0.081 (1)	-0.081	0.030
H101.6×101.6×6.35-C	-35.48		-37.61	1.34	-87.98	-0.046 (1)	-	-0.083 (1)	-	-0.083	0.037
N101.6×50.8×3.25	9.61	49% (-)	9.99	1.55	66.84	0.026 (1)	-	0.064 (1)	-0.067 (1)	0.070	0.030
N101.6×50.8×3.25-C	-13.24		-13.90	1.66	-69.74	-0.023 (1)	-	-0.066 (1)	-0.072 (2)	-0.077	0.049
N76.2×76.2×3.25	-9.04	22% (+)	-9.58	2.02	-86.58	-0.037 (1)	0.056 (2)	-0.082 (1)	-	-0.082	0.045
N76.2×76.2×3.25-C	-9.62		-10.20	1.59	-80.93	-0.028 (1)	0.064 (2)	-0.076 (1)	-0.081 (1)	0.080	0.053

* The sign in the parentheses indicates positive or negative direction. ** The number in the parentheses indicates 1st or 2nd cycle of the mentioned amplitudes.

*** Calculated as $(F_{max,CFAT}-F_{max,BAT})/F_{max,BAT}$

Table 4. (continued).

Specimen ID	Ductility coefficient, μ	Plastic hinge length, L_{PH} (mm)	L_{PH}/D
H152.4×50.8×6.35	1.62	203	1.33
H152.4×50.8×6.35-C	2.04	236	1.54
H101.6×101.6×6.35	1.50	143	1.41
H101.6×101.6×6.35-C	1.80	192	1.89
N101.6×50.8×3.25	2.46	140	1.38
N101.6×50.8×3.25-C	2.89	151	1.49
N76.2×76.2×3.25	2.21	103	1.35
N76.2×76.2×3.25-C	2.73	120	1.58
Mean			1.50
COV			0.11

Nonlinear cyclic response of concrete-filled aluminium beam members (component response)

General observations

The obtained $F–\delta$ and $M–\theta$ hysteretic and envelope curves, along with photographs for all concrete-filled aluminium beam members at the completion of the tests are shown in Figs. 9-12. In general, the observed damage mechanisms were similar to those obtained for the hollow beam members.

Classes 1 and 2 6082-T6 cross-sections

The H152.4×50.8×6.35-C specimen failed beyond 0.06 rad with two fractures developed in the vicinity of the top hole (see Fig. 9(c)), while the H101.6×101.6×6.35-C specimen sustained the maximum applied θ of -0.083 rad.

Classes 2 and 3 6063-T6 cross-sections

The N101.6×50.8×3.25-C specimen failed similarly to H152.4×50.8×6.35-C specimen, as shown in Fig.11(c). The N76.2×76.2×3.25-C specimen achieved its M_{max} at -0.076 rad and failed in the subsequent amplitude due to a fracture initiated at the tip of the steel angles (see Fig. 10(c)). For the N76.2×76.2×3.25-C specimen, visual inspection showed consistent results with the hysteretic behaviour, where minor local buckling around the corners at large θ levels (>0.06 rad) was visible. This behaviour is significantly improved compared to the corresponding hollow N76.2×76.2×3.25 specimen, which is expected, as the concrete infill prevents inward/delays outward local buckling of the aluminium tube (Georgantzia et al. 2021a).

Comparison of all hollow and concrete-filled members

To compare the hysteretic behaviour of all tested members, the normalised $M–\theta$ envelope curves are plotted at the same graph as shown in Fig. 13. The M was normalised with the theoretical plastic moment capacity M_{pl} calculated according to EN 1999-1-1 (CEN 2023a) for the hollow beam members and EN 1999-1-1 (CEN 2023a) combined with the EN 1994-1-1 (CEN 2023b) for the concrete-filled members (as suggested in Georgantzia et al. 2021a). The absolute values of the normalised maximum bending moment $|M_{max}/M_{pl}|$ are also included in Table 4. It can be observed that the slope of the normalised $M–\theta$ envelope curves corresponding to concrete-filled specimens is relatively larger suggesting higher stiffness. Furthermore, to quantify the influence of the concrete infill on the F_{max}, the percentage increase was calculated and added to Table 4. The results indicate that the presence of the concrete infill

enhanced the lateral load capacity of all specimens, with improvements ranging from 12% to 49%. Moreover, the plastic rotation θ_{pl} values for all beam members were calculated and listed in Table 4, showing that the concrete infill significantly enhances the deformability of the plastic hinge region.

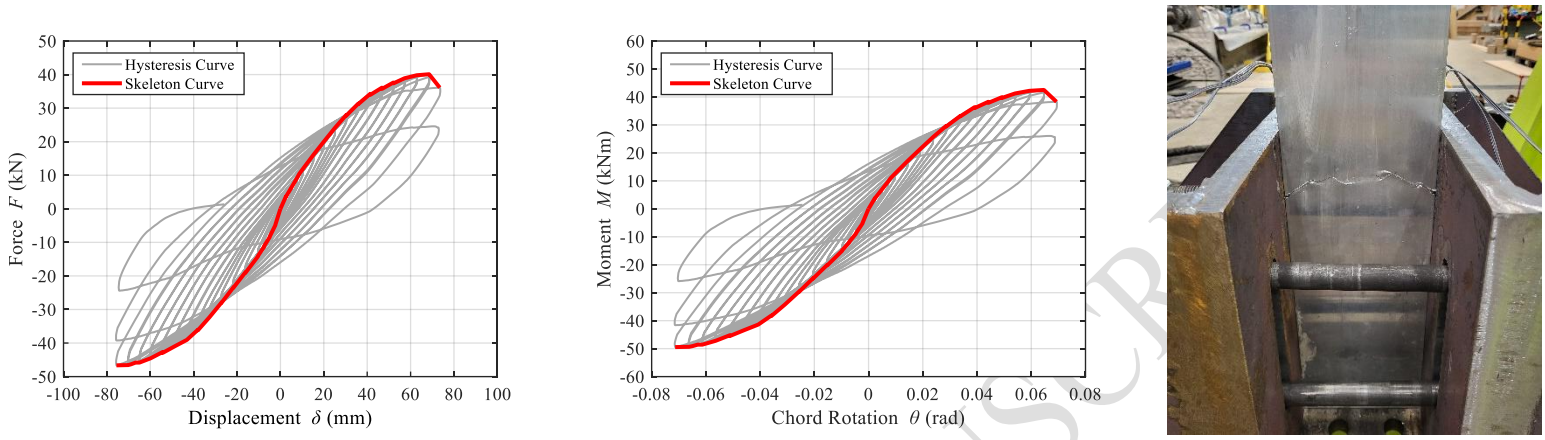

(a) (b) (c)

Fig. 9: Nonlinear cyclic response of the H152.4×50.8×6.35-C beam; (a) force-displacement hysteretic curve, (b) moment-chord rotation hysteretic curve and (c) photograph of the specimen at completion of the test.

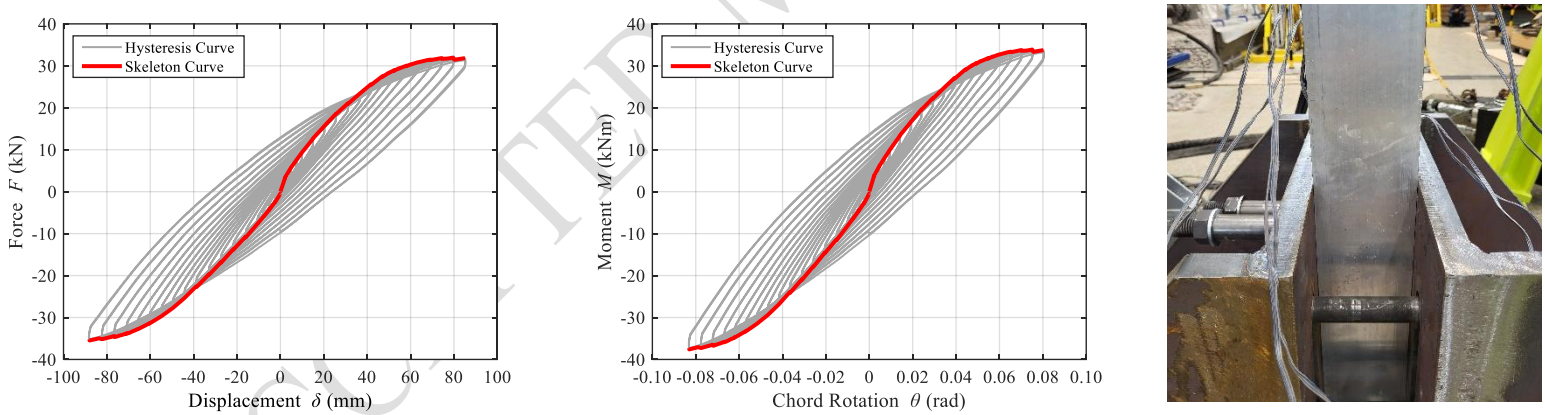

(a) (b) (c)

Fig. 10: Nonlinear cyclic response of the H101.6×101.6×6.35-C beam; (a) force-displacement hysteretic curve, (b) moment-chord rotation hysteretic curve and (c) photograph of the specimen at completion of the test.

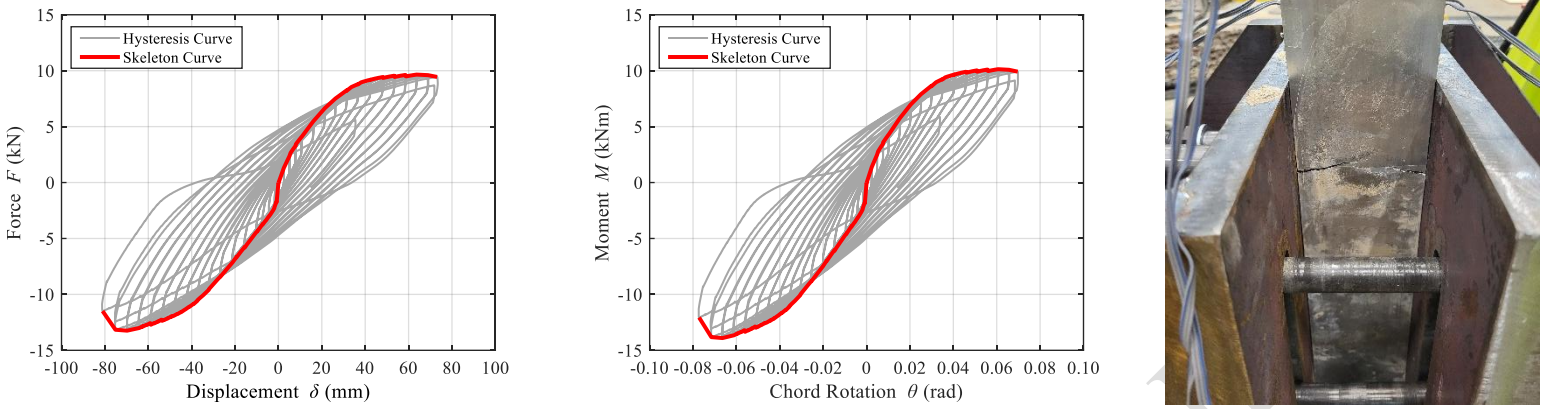

(a) (b) (c)

Fig. 11: Nonlinear cyclic response of the N101.6×50.8×3.25-C beam; (a) force-displacement hysteretic curve, (b) moment-chord rotation hysteretic curve and (c) photograph of the specimen at completion of the test.

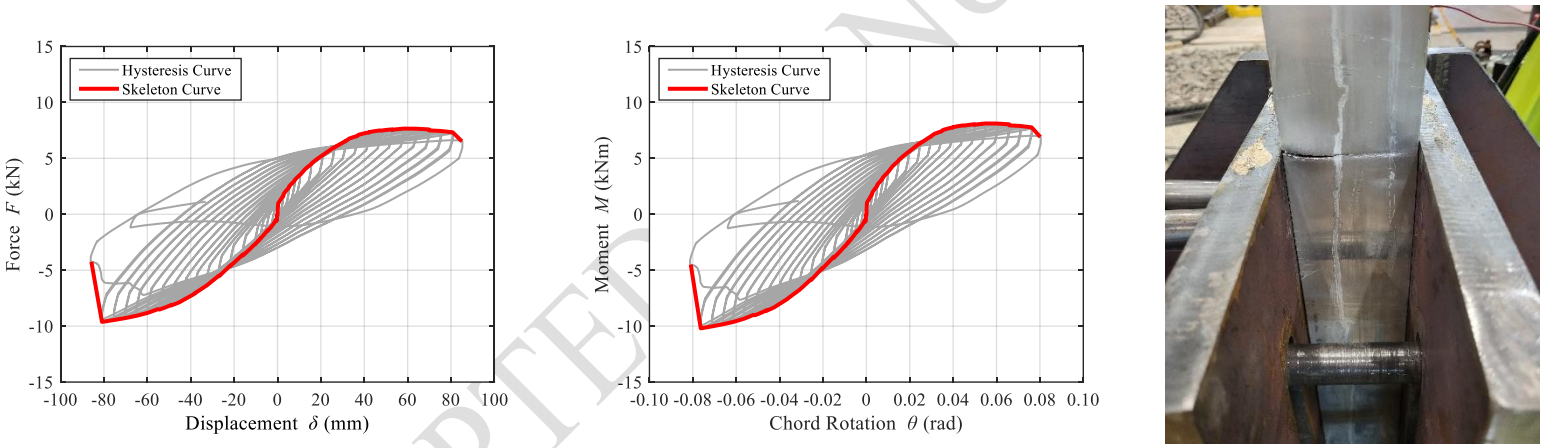

(a) (b) (c)

Fig. 12: Nonlinear cyclic response of the N76.2×76.2×3.25-C beam; (a) force-displacement hysteretic curve, (b) moment-chord rotation hysteretic curve and (c) photograph of the specimen at completion of the test.

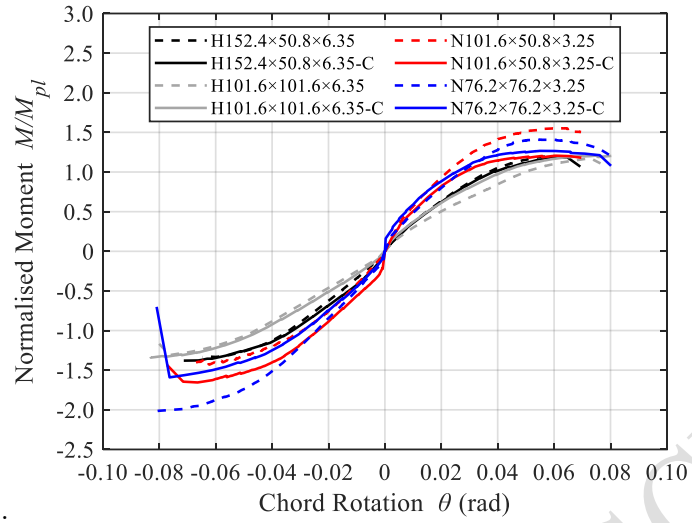

Fig. 13: Normalised moment-chord rotation envelope curves at completion of the tests for all beam members.

Moment-Curvature hysteretic response of hollow and concrete-filled aluminium beam members (cross-section response)

Figs. 14 and 15 show the moment–curvature (M–φ) hysteretic curves of all beam members. The M was calculated as $F{\cdot}L_{eff}$ while the φ was estimated using the following equation from (Kashani et al. 2024):

$$\phi = (\varepsilon_t - \varepsilon_c)/D \quad \text{(1/mm)} \tag{2}$$

where ε_t and ε_c are the extreme fibre tensile and compressive strains, respectively, measured at the cross-section located 10 mm distance from the tip of the steel angles. It is noted that only the reasonable recorded strain results (corresponding to a maximum θ between 0.04 rad and 0.08 rad) were used to plot the M–φ hysteretic curves.

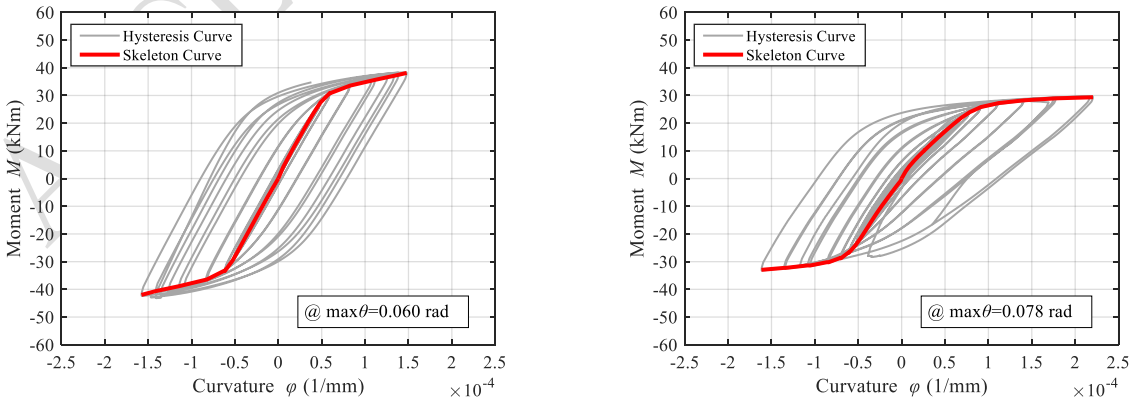

(a) (b)

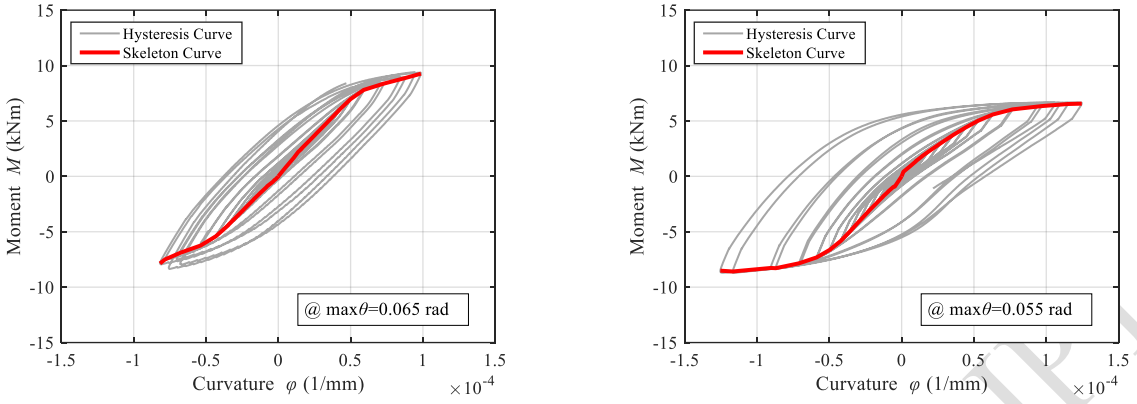

(c) (d)

Fig. 14: Moment-curvature hysteretic curves of the hollow aluminium beam members; (a) H152.4×50.8×6.35, (b) H101.6×101.6×6.35, (c) N101.6×50.8×3.25 and (d) N76.2×76.2×3.25.

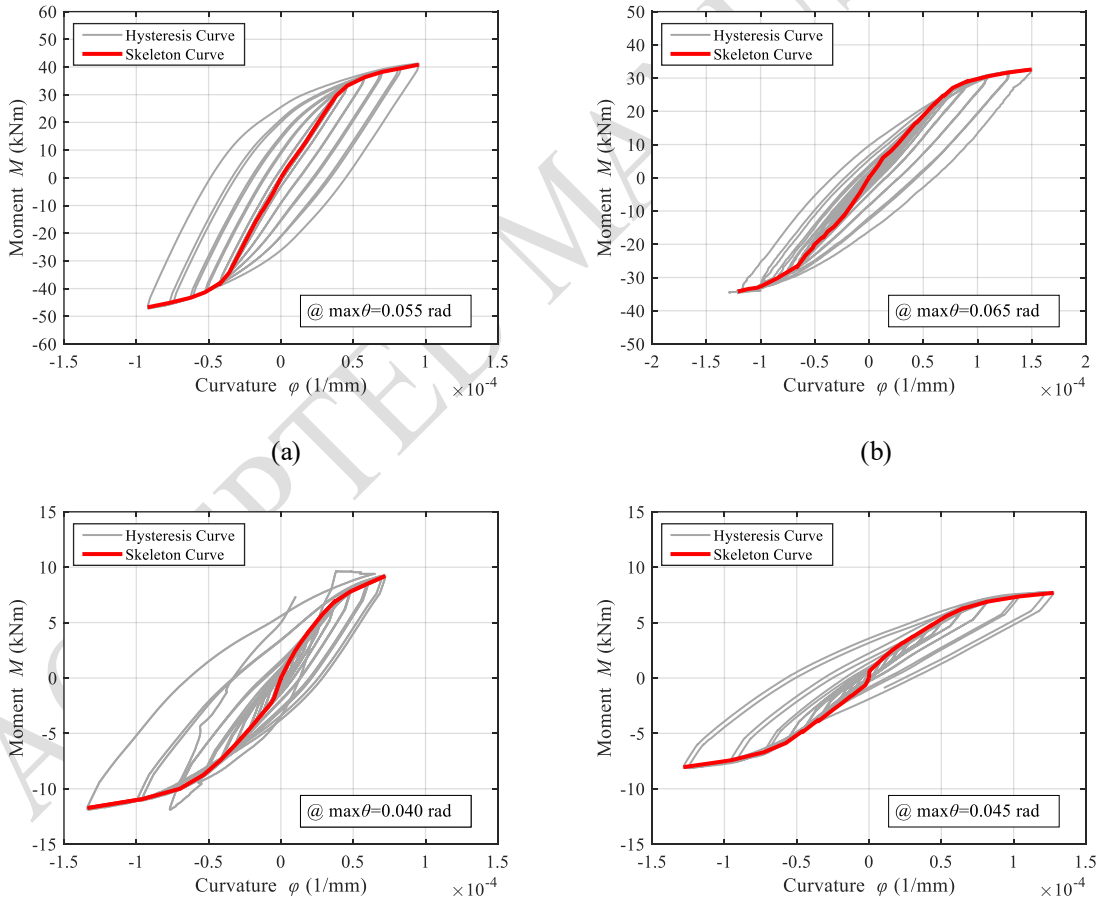

(a) (b)

(c) (d)

Fig. 15: Moment-curvature hysteretic curves of the concrete filled aluminium beam members; (a) H152.4×50.8×6.35-C, (b) H101.6×101.6×6.35-C, (c) N101.6×50.8×3.25-C and (d) N76.2×76.2×3.25-C.

To directly compare the hysteretic behaviour of all beam members, normalised M–φ envelope curves corresponding to a maximum θ=0.04 rad are plotted together in Fig. 16. It is evident that the 6063-T6 sections (plotted with red and blue colour) infilled with concrete or not, exhibit higher normalised bending moment capacities throughout the considered θ range. Particularly, the M_{pl} is being exceeded by up to 50% compared to that of their 6082-T6 counterparts (plotted with black and grey colour). This is related to the higher strain hardening properties of 6063-T6, i.e., lower strain hardening exponent n, which results in higher tangent stiffness in the inelastic range enabling for higher normalised bending moment capacities.

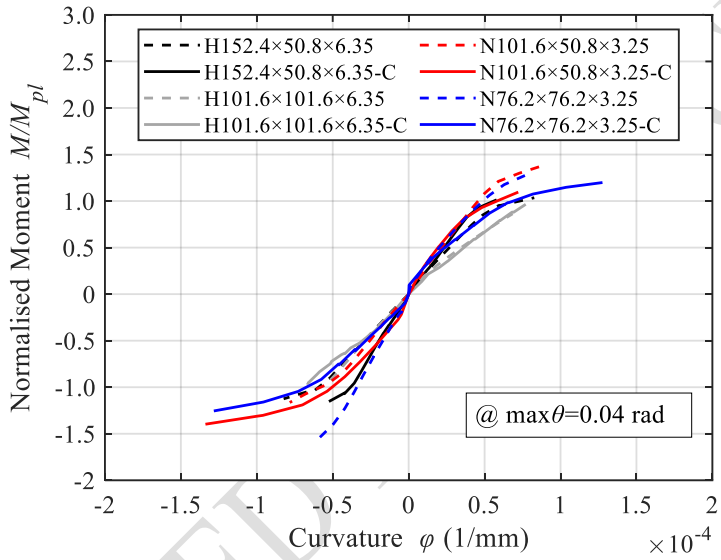

Fig. 16: Normalised moment-curvature envelope curves corresponding to maximum chord rotation of 0.04 rad for all tested beam members.

Secant Stiffness degradation

The mean secant stiffness K_{sec} of all members for each cycle is estimated as follows:

$$K_{\text{sec}} = \frac{\left|F^{+}_{\text{max},i}\right| + \left|F^{-}_{\text{max},i}\right|}{\left|\delta^{+}_{\text{max},i}\right| + \left|\delta^{-}_{\text{max},i}\right|} \quad \text{(kN/m)} \tag{3}$$

where F_{max} and δ_{max} is the peak force and peak displacement, respectively, in positive and negative direction for each cycle.

To compare the stiffness degradation of all hollow members, the K_{sec} calculated for each cycle in each beam was normalised to the initial K_{sec} at the 1st cycle. For the concrete-filled members, the K_{sec} calculated for each cycle in each

beam was normalised to the initial K_{sec} at the 1st cycle of the hollow member with the same cross-section. This allows to assess the influence of the concrete infill on the stiffness degradation. Fig. 17 shows the normalised mean secant stiffness $K_{sec}/K_{sec,First,BAT}$ over the cycle number of all tested beam members. Generally, all hollow members exhibited relatively stable stiffness degradation, with no significant differences observed among them, except from the H101.6×101.6×6.35 specimen, which showed less stiffness loss after the 12th cycle. Moreover, the graph shows that concrete-filled members have higher initial stiffness compared to their hollow counterparts, though the extent of this difference depends on the cross-section thickness. Particularly, the initial stiffness of the H152.4×50.8×6.35-C and H101.6×101.6×6.35-C specimens was 30% and 35% higher, respectively, while for the N101.6×50.8×3.25-C and N76.2×76.2×3.25-C specimens, it was 77% and 50%, respectively. This is because the latter two specimens comprise cross-sections with thinner plate elements, which increases the proportion of concrete infill in the total cross-section, resulting in higher initial stiffness. However, as the lateral displacement increases during testing, the rate of stiffness degradation in concrete-filled members exceeds that of the hollow members. This is attributed to the damage in the concrete infill, which becomes more significant as the loading increases. It is noted that the H101.6×101.6×6.35-C specimen, after the 12th cycle –like its hollow counterpart–, exhibited less stiffness degradation compared to the other concrete-filled members. Overall, the stiffness degradation of all members at the completion of tests ranged between 50% and 77%.

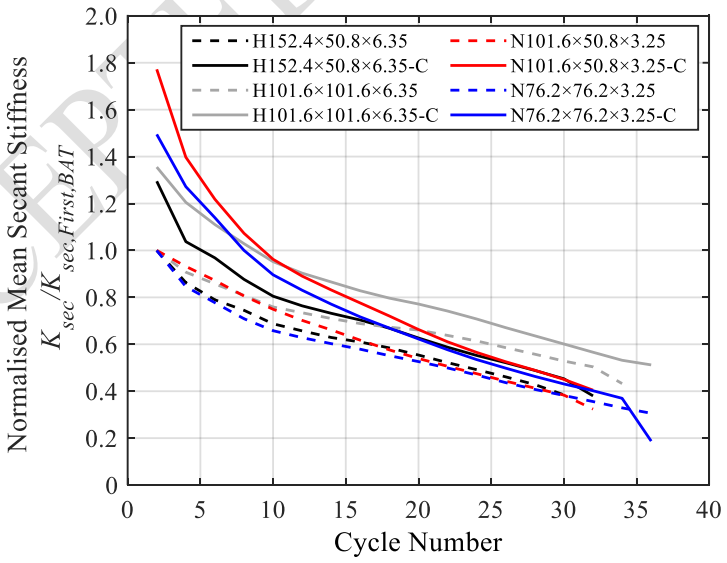

Fig. 17: Normalised mean secant stiffness of all tested beam members.

Ductility and energy dissipation capacity

Ductility coefficient μ provides a measure of a member's ability to undergo deformation beyond its elastic limit while maintaining a significant load-carrying capacity up to the point of failure. Depending on the type of structural member being referred to, the deformation used to evaluate ductility can be strain, curvature, displacement or rotation. In the current case of hollow and concrete-filled aluminium beams, the chord rotation is the most suited deformation. Thus, μ was calculated for each beam member as the ratio of $\theta_{max}/\theta_{0.2}$ and the resulting values are listed in Table 4. Higher μ values were achieved in members comprising aluminium tubes from 6063-T6 normal strength alloy which exhibits slightly higher ε_f compared to stronger 6082-T6 (see Table 2). Overall, all test specimens demonstrated satisfactory ductility with corresponding μ values ranging from 1.50 to 2.89. However, these values would have been higher if the specimens' support conditions were fully fixed, which would result in lower elastic rotation $\theta_{0.2}$.

Another important index to evaluate the nonlinear cyclic performance of structural components is energy dissipation capacity. In this paper, the cumulative hysteretic energy of each specimen was calculated for each amplitude as the area enclosed by the two hoops from the F–δ hysteretic curves. Then, the calculated cumulative hysteretic energy was normalised to the corresponding total hysteretic energy dissipated during testing and was plotted against the number of cycles, as shown in Figs. 18 and 19. For both hollow and concrete-filled members, the graphs show that there was minimal energy dissipation until the 12th cycle (corresponding to θ=0.02 rad and δ=20 mm), which is in line with the secant stiffness degradation results illustrated in Fig. 17. This indicates that at this loading level, the behaviour remains within the elastic range, with no initiation of damage mechanisms (concrete cracking and aluminium yielding).

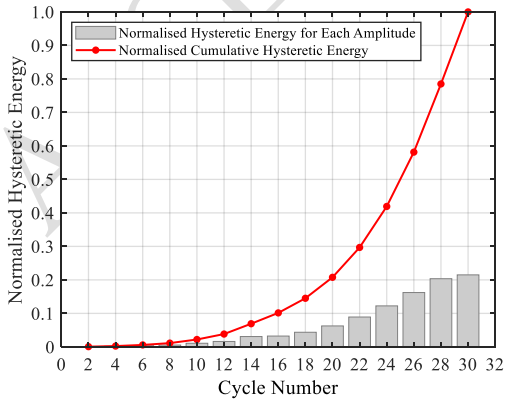

(a)

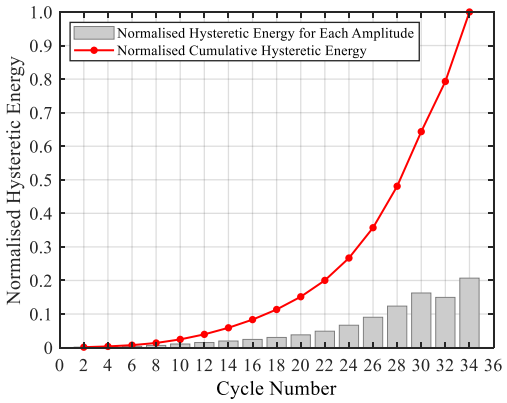

(b)

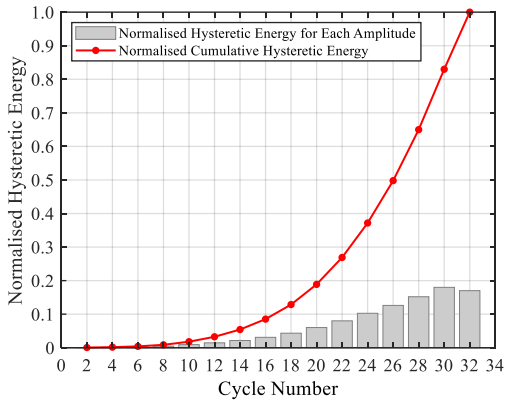

(c)

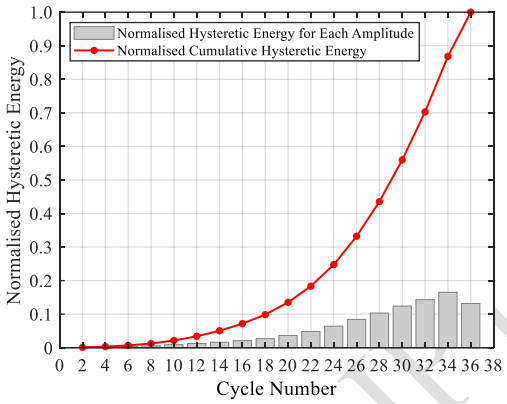

(d)

Fig. 18: Hysteretic energy dissipation of the hollow aluminium beam members; (a) H152.4×50.8×6.35, (b) H101.6×101.6×6.35, (c) N101.6×50.8×3.25 and (d) N76.2×76.2×3.25.

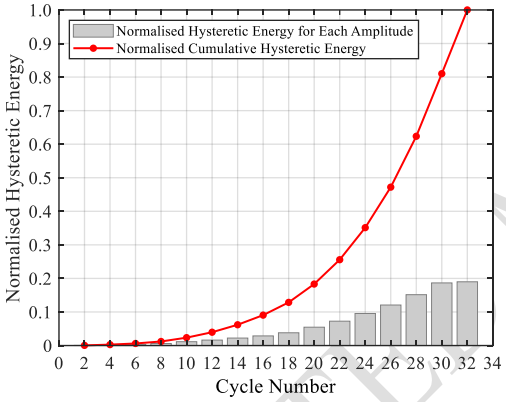

(a)

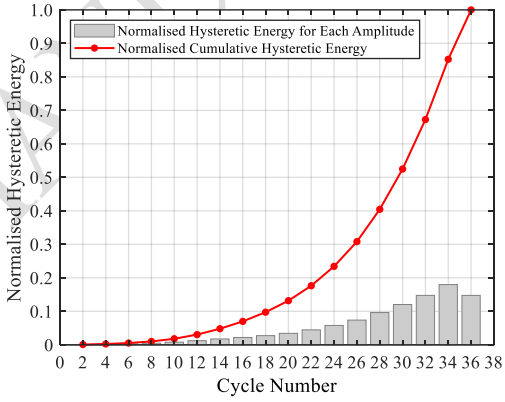

(b)

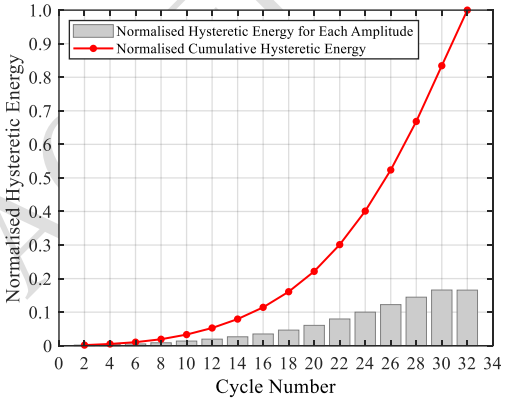

(c)

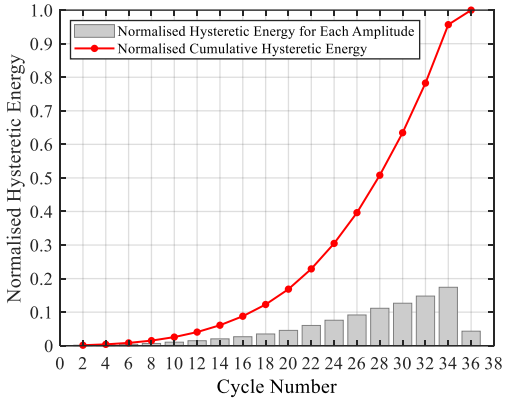

(d)

Fig. 19: Hysteretic energy dissipation of the concrete-filled aluminium beam members; (a) H152.4×50.8×6.35-C, (b) H101.6×101.6×6.35-C, (c) N101.6×50.8×3.25-C and (d) N76.2×76.2×3.25-C.

To compare the energy dissipation capacity of all tested members, their normalised cumulative hysteretic energy dissipation is shown in Fig. 20. As expected, the results showed that at later cycles, the cumulative hysteretic energy is highest for the H152.4×50.8×6.35 specimen which failed at lowest θ level. Conversely, the H101.6×101.6×6.35-C specimen which sustained the maximum applied θ without presenting any severe structural damage, achieved the smallest cumulative hysteretic energy values. For example, at the 30th cycle and when the H152.4×50.8×6.35 specimen fractured, the H101.6×101.6×6.35-C specimen had dissipated roughly the 53% of its total hysteretic energy (attributed to concrete infill cracking).

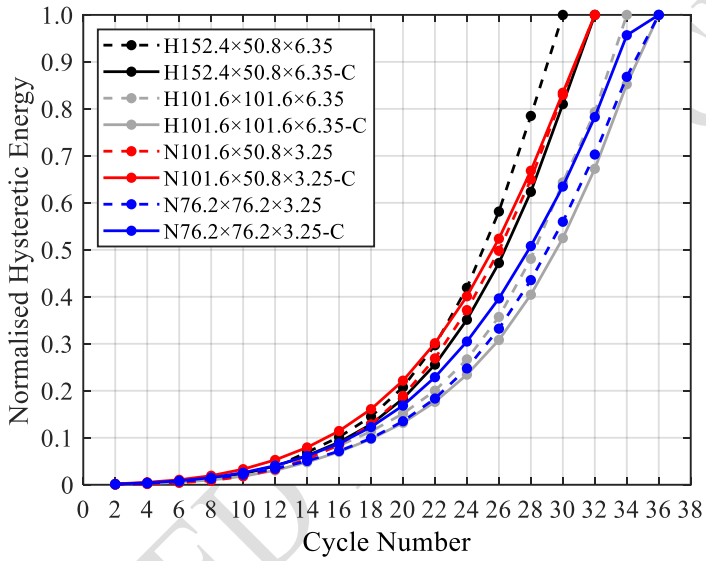

Fig. 20: Hysteretic energy dissipation of all tested beam members.

Plastic hinge length estimation

The strain measurements from the DIC were used to analyse the strain distribution along the web and estimate the associated plastic hinge length L_{PH} of each member. The strains recorded at discrete sample points by the gauges, were utilised to verify the plausibility of the DIC strain measurements. The analysis showed that yielding was propagating over a larger member length, as the rotation level was increasing up to roughly θ=0.04 rad. Beyond this point the plastic strain evolution localised near the member's fixed end. It is noted that in this study, the fixed end is either at the tip of the steel angles or the top hole of the specimen. Fig. 21 illustrates the average strain distribution on both sides at the bottom end of four typical beam members at characteristic chord rotations –1st cycle of each amplitude–, as measured by the DIC system. The L_{PH} was determined as the distance between the furthest cross sections along the

member length at which the longitudinal strain exceeded the proof strain $\varepsilon_{0.02}$, i.e., strain corresponding to $\sigma_{0.02}$. Table 4 summarises the L_{PH} of all tested beam members. The L_{PH} values were normalised with respect to the cross-sectional depth D of each member. The normalised L_{PH} values were added to Table 4 along with the corresponding mean and COV values. Overall, the findings suggest that the considered cross-sections can sustain large cyclic loads with an average associated L_{PH} equal to $1.5D$ measured from the fixed end. Fig. 22 which shows DIC contour plots of Von Mises equivalent strains of typical beam members at θ level corresponding to M_{max}, confirms that most of the inelastic deformation was concentrated around these areas.

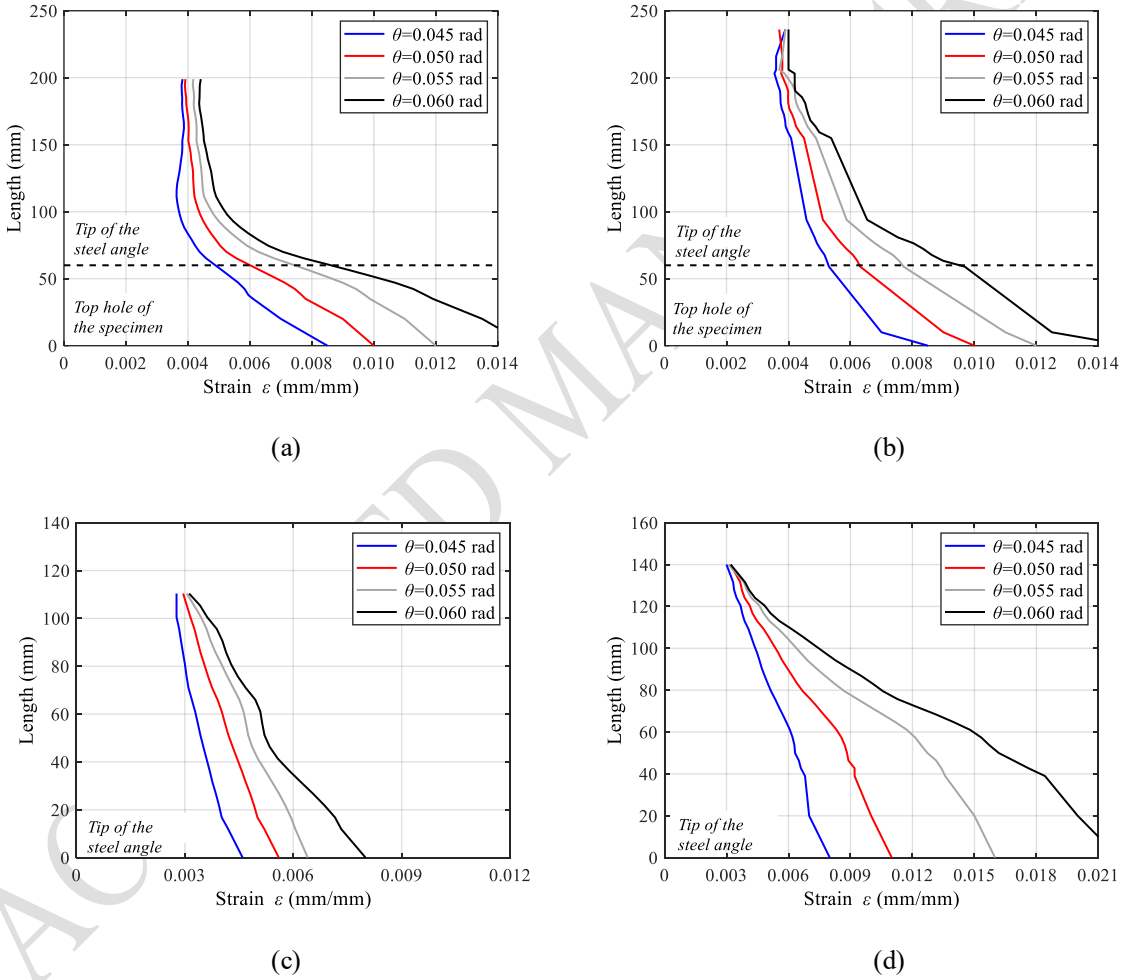

Fig. 21: Strain distribution at the bottom end of typical beam members at characteristic chord rotations (1st cycle of each amplitude); (a) H152.4×50.8×6.35, (b) H152.4×50.8×6.35-C, (c) N76.2×76.2×3.25 and (d) N76.2×76.2×3.25-C.

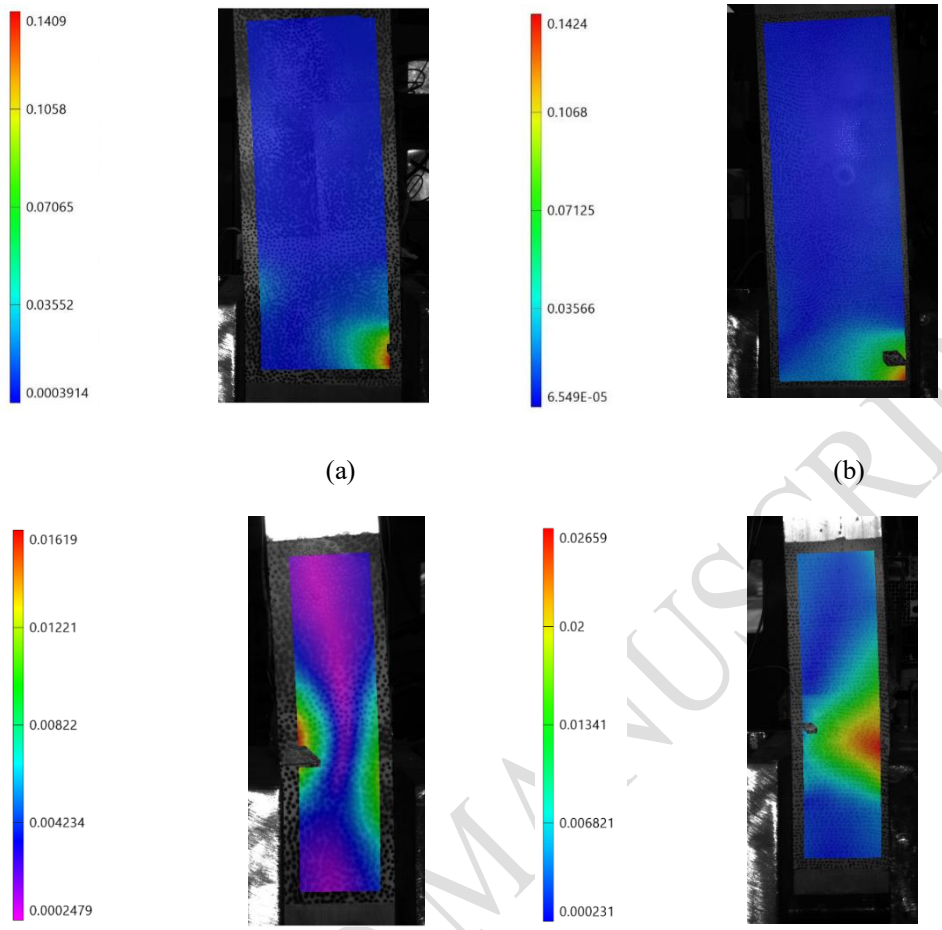

Fig. 22

: Representative DIC contour plots of Von Mises equivalent strains of typical beam members at rotation level corresponding to maximum bending moment (1st cycle of this amplitude); (a) H152.4×50.8×6.35, (b) H152.4×50.8×6.35-C, (c) N76.2×76.2×3.25 and (d) N76.2×76.2×3.25-C.

Practical applications and limitations

This paper presents unique experimental data on the inelastic cyclic performance of hollow and concrete-filled aluminium beam members, examining the effects of alloy type, cross-sectional slenderness, and concrete infill on plastic hinge deformation, ultimate strength, failure mode, stiffness degradation, and energy dissipation. The study includes four Class 1-3 (CEN 2023a) tubular sections made from 6082-T6 and 6063-T6 alloys and with a maximum size of 152 mm. Although the dimensions are small for use in primary flexural members in typical building applications, they enabled a detailed investigation into the fundamental structural behaviour of hollow and concrete-filled aluminium beams under cyclic loading. Moreover, the obtained results provide a reliable basis for scaling up

through validated numerical models and built-up sections. While the findings are compelling, they are based on a limited dataset and thus require further validation. Future studies –including additional testing and broader parametric investigations– should explore a broader range of cross-section slenderness, alloys, concrete strengths, and loading protocols to draw generalised conclusions and suggest design recommendations.

Concluding remarks

The objective of this study was to characterise the cyclic major-axis flexural behaviour of hollow and concrete-filled sections and evaluate their potential for use in building applications in seismic-prone zones. To this end, four Class 1-3 (CEN 2023a) tubular cross-sections, fabricated from two aluminium alloys –6082-T6 and 6063-T6– were used to form 1500 mm-long members. The aluminium members were tested as hollow and concrete-filled under large inelastic bending cycles and their resulting hysteretic behaviour was thoroughly analysed. The major conclusions derived from this study are summarised as follows:

- All tested specimens displayed symmetrical hysteretic loops without significant gradual strength degradation under cyclic loading, and failed at large θ levels between 0.064 rad and 0.081 rad.
- In hollow aluminium members, yielding initiated between 0.023 rad and 0.051 rad depending on the alloy type and cross-section size, and damage was localised at the bottom end of the specimens around the top hole. Among specimens fabricated from the same alloy, failure occurred earlier in those with larger cross-sectional dimensions due to their higher stiffness, which corresponded to smaller θ. Moreover, specimens with larger cross-sectional dimensions and fabricated from high-strength 6082-T6 alloy achieved higher M_{max}.
- Chapter 15 in the latest draft of the Second Generation of EN1998-1-2 (CEN 2022), allows only Class 1 cross-sections to be used for dissipative aluminium members in bending and only for ductility class DC2. In this study, it was found that the plastic hinge region of beam members with Class 2 and 3 cross-sections, provide plastic rotation capacity θ_{pl} higher than 0.02 rad (value adopted from Chapter 11 for steel structures). Therefore, Class 2 and 3 cross-sections can be used for dissipative aluminium members in bending in DC2 buildings.
- The 6082-T6 and 6063-T6 alloys investigated in this study can be considered for inclusion in Chapter 15 as permitted alloys for dissipative members in DC2 buildings.
- For the concrete-filled aluminium members, the hysteretic responses were quite good and the observed damage mechanisms were similar to those obtained for their hollow counterparts. However, in the Class 3 section

member, the concrete infill successfully prevented inward and delayed outward local buckling of the aluminium tube. Relative comparisons indicated that the concrete infill in the concrete-filled aluminium specimens significantly enhanced the deformability of the plastic hinge region, and increased the lateral load capacity by 12% to 49%.

- Normalised M–φ envelope curves corresponding to a θ=0.04 rad showed that the 6063-T6 sections infilled with concrete or not, exhibit higher normalised bending moment capacities throughout the considered θ range. Particularly, the M_{pl} is being exceeded by up to 50% compared to that of their 6082-T6 counterparts.
- The initial stiffness of members with concrete-filled sections, particularly those with thinner plate elements, is higher than that of the corresponding ones with hollow sections. However, as the lateral displacement increases, the rate of stiffness degradation in concrete-filled aluminium members exceeds that of the hollow members. This is attributed to the damage in the concrete infill, which becomes more significant as the loading increases. Overall, the stiffness degradation of all members at the completion of tests ranged between 50% and 77%.
- All members demonstrated satisfactory ductility with corresponding μ values ranging from 1.50 to 2.89. However, these values would be higher if the specimens' support conditions were fully fixed, which would result in lower $\theta_{0.2}$.
- Analyses of the strain measurements from the DIC system suggest that the examined members can sustain large cyclic loads with an average associated plastic hinge length L_{PH} equal to 1.5D measured from the fixed end.
- The reported performance data serve as a valuable foundation for future numerical modelling studies, which can provide deeper insights and support the development of a practical design framework for hollow and concrete-filled aluminium members subjected to large cyclic bending loads.

In conclusion, the cyclic flexural tests conducted in this study demonstrate the favourable inelastic cyclic performance of hollow and concrete-filled aluminium beam members, indicating their ability to sustain large deformation without any structural damage under high rotation levels (beyond 0.064 rad). This high efficiency at structural damage is due to aluminium's low modulus of elasticity –approximately one-third that of steel– which keeps further the structural members and thereby the entire structure into the elastic region –more flexible structure– and postpones yield occurrence at higher rotation levels. However, this can be dealt with during the design of structural systems. For instance, a moment resisting frame alone may not be suitable for aluminium structures due to low elastic modulus of the material, but by adding bracing to the whole structural system can be stiffened. Therefore, there is a

need for extensive research in the future to realise the full potential of aluminium as structural material to be used in seismic design.

Data availability

Some or all data, models, or code that support the findings of this study are available from the corresponding author upon reasonable request.

Acknowledgements

The experiments were performed in the LSTL within the National Infrastructure Laboratory, part of the UK Collaboratorium for Research on Infrastructure and Cities, based at the University of Southampton. The help of Mr Andrew Morgan, LSTL Technician, in preparing the test specimens is gratefully acknowledged.

References

"ABAQUS Standard user's manual. Providence, RI: Dassault Systèmes Simulia Corp."

AA. (The Aluminum Association): 2020. Aluminum Design Manual. Washington, DC, USA, 2020.

Ali, S. Bin, G. S. Kamaris, M. Gkantou, and K. D. Kansara. 2022. "Concrete-filled and bare 6082-T6 aluminium alloy tubes under in-plane bending: Experiments, finite element analysis and design recommendations." *Thin-Walled Struct.* 172. https://doi.org/10.1016/j.tws.2022.108907.

Araújo, M., and J. M. Castro. 2016. "On the quantification of local deformation demands and adequacy of linear analysis procedures for the seismic assessment of existing steel buildings to EC8-3." *Bull. Earth. Eng.* 14 (6): 1613–1642. https://doi.org/10.1007/s10518-016-9897-4.

AIJ. (Architectural Institute of Japan). 2003. *Recommendation for Seismic Design of Aluminium Structures*. Tokyo, Japan (In Japanese).

Bock, M., M. Theofanous, S. Dirar, and N. Lipitkas. 2021. "Aluminium SHS and RHS subjected to biaxial bending: Experimental testing, modelling and design recommendations." *Eng Struct*, 227. https://doi.org/10.1016/j.engstruct.2020.111468.

Castaldo, P., E. Nastri, and V. Piluso. 2017. "Ultimate behaviour of RHS temper T6 aluminium alloy beams subjected to non-uniform bending: Parametric analysis." *Thin-Walled Struct.* 115: 129–141. https://doi.org/10.1016/j.tws.2017.02.006.

CEN (European Committee for Standardization). 2004. *Design of Concrete Structures. Part 1-1: General rules and rules for buildings*. Brussels, Belgium: CEN.

CEN (European Committee for Standardization). 2023a. *Eurocode 9: design of aluminium structures. Part 1-1: General structural rules.* BS EN 1999-1-1:2023. Brussels, Belgium: CEN.

CEN (European Committee for Standardization). 2023b. *Eurocode 4: design of composite steel and concrete structures. Part 1-1: General structural rules and rules for buildings.* BS EN 1994-1-1:2023. Brussels, Belgium: CEN.

CEN (European Committee for Standardization). 2019a. *Metallic Materials - Tensile testing-Part 1: Method of test at room temperature.* BS EN ISO 6892-1:2019. Brussels, Belgium: CEN.

CEN (European Committee for Standardization). 2019b. *Testing fresh concrete-Part 2: Slump test.* BS EN 12350-2:2019. Brussels, Belgium: CEN.

CEN (European Committee for Standardization). CEN/TC 250/SC 8. 2022. *Design of Structures for Earthquake Resistance. Part 1-2: General Rules and Seismic Action*. BS EN 1998-1-2:2022. Brussels, Belgium: CEN.

Chen, Y., R. Feng, and W. Gong. 2018. "Flexural behavior of concrete-filled aluminum alloy circular hollow section tubes." *Constr. Build. Mater*. 165: 173–186. https://doi.org/10.1016/j.conbuildmat.2017.12.104.

Chen, Y., R. Feng, and J. Xu. 2017. "Flexural behaviour of CFRP strengthened concrete-filled aluminium alloy CHS tubes." *Constr. Build. Mater*, 142: 295–319. https://doi.org/10.1016/j.conbuildmat.2017.03.040.

Feng, R., Y. Chen, and W. Gong. 2017. "Flexural behaviour of concrete-filled aluminium alloy thin-walled SHS and RHS tubes." *Eng. Struct.* 137: 33–49. https://doi.org/10.1016/j.engstruct.2017.01.036.

Georgantzia, E., and M. Gkantou. 2021. "Flexural Buckling of Concrete-Filled Aluminium Alloy CHS Columns: Numerical Modelling and Design." In Advances in Geotechnics and Structural Engineering: Select Proc. of TRACE 2020. *Lecture Notes in Civil Engineering*, 143. 697-707. https://doi.org/10.1007/978-981-33-6969-6_61.

Georgantzia, E., S. Bin Ali, M. Gkantou, G. S. Kamaris, K. D. Kansara, and W. Atherton. 2021a. "Flexural buckling performance of concrete-filled aluminium alloy tubular columns." *Eng. Struct*. 242. https://doi.org/10.1016/j.engstruct.2021.112546.

Georgantzia, E., M. Gkantou, G. S. Kamaris, and K. D. Kansara. 2022a. "Ultimate response and plastic design of aluminium alloy continuous beams." *Structures.* 39: 175–193. https://doi.org/10.1016/j.istruc.2022.03.015.

Georgantzia, E., S. Bin Ali, M. Gkantou, G. S. Kamaris, P. Kot, and K. S. Hashim. 2022b. "Numerical modelling of concrete-filled aluminium alloy 6082-T6 columns under axial compression." *J Phys Conf Ser*. 2198. https://doi.org/10.1088/1742-6596/2198/1/012045.

Georgantzia, E., M. Gkantou, G. S. Kamaris, and K. D. Kansara. 2022c. "Design of aluminium alloy channel sections under minor axis bending." *Thin-Walled Struct.* 174 https://doi.org/10.1016/j.tws.2022.109098

Georgantzia, E., M. Gkantou and G. S. Kamaris 2023. "Aluminium alloy channel columns: Testing, numerical modelling and design." *Thin-Walled Struct.* 182 https://doi.org/10.1016/j.tws.2022.110242

Georgantzia, E., C. Finney, A. F. Robinson, and M. M. Mehdi Kashani. 2024. "Modeling Nonlinear Stress-Strain Behavior of 6000 Series Aluminum Alloys under Cyclic Loading." *J. Mater. Civ. Eng.* 36 (6) https://doi.org/10.1061/JMCEE7.MTENG-17314.

Georgantzia, E., and M. M. Mehdi Kashani. 2024. "On the use of aluminium alloys in sustainable design, construction, and rehabilitation of bridges: emerging applications and future opportunities." *Proceedings of the Institution of Civil Engineers: Bridge Engineering*. https://doi.org/10.1680/jbren.23.00018.

Gkantou, M., E. Georgantzia, A. Kadhim, G. S. Kamaris, and M. Sadique. 2023. "Geopolymer concrete-filled aluminium alloy tubular cross-sections." *Structures*, 51. https://doi.org/10.1016/j.istruc.2023.02.117.

Hill, H. N., J. W. Clark, and R. J. Brungraber. 1960. "Design of Welded Aluminum Structures." *J. Struct. Div.* 86 (6): 101–124. https://doi.org/10.1061/JSDEAG.0000524.

Kashani, M. M., H. Moodley, H. O. Aminulai, S. Afshan, and D. Crump. 2024. "Experimental Investigation of Nonlinear Cyclic Behavior of Circular Concrete Bridge Piers with Pitting Corrosion." *J. Bridge Eng.* 29 (8). https://doi.org/10.1061/jbenf2.beeng-6482.

Krawinkler, H., A. Gupta, R. Medina, and N. Luco. 2000. *Development of loading histories for testing of steel beam-to-column assemblies.* Washington, DC: FEMA.

Nastri, E., V. Piluso, A. Pisapia, F. Pisciottano, and P. Todisco. 2025. "First exploring the cyclic behaviour of aluminium beams under non-uniform bending: Experimental and FE analysis." *Eng Struct*, 322. https://doi.org/10.1016/j.engstruct.2024.119144.

Piluso, V., A. Pisapia, E. Nastri, and R. Montuori. 2019. "Ultimate resistance and rotation capacity of low yielding high hardening aluminium alloy beams under non-uniform bending." *Thin-Walled Struct.* 135: 123–136. https://doi.org/10.1016/j.tws.2018.11.006.

Ramberg, W., and W. Osgood. 1943. "Description of stress-strain curves by three parameters. Vol. Technical." *Washington, DC: National Advisory Committe for Aeronautics.*

Su, M.N., Young, B. and Gardner, L. 2014. "Deformation-based design of aluminium alloy beams." *Eng. Struct.* 80: 339–49. https://doi.org/10.1016/j.engstruct.2014.08.034

Zhu, J.H. and Young, B. 2009. "Design of aluminum alloy flexural members using direct strength method." *J. Struct. Eng.* 135(5): 558–66. https://doi.org/10.1061/(ASCE)ST.1943-541X.000000